RSC Advances

ROYAL SOCIETY OF CHEMISTRY

www.rsc.org/advances

Cite this: DOI: 10.1039/c0xx00000x

www.rsc.org/xxxxxx

ARTICLE TYPE

Hydrocarbon Chain Growth and Hydrogenation on V(100): A Density Functional Theory Study

Hui Wang,[a] Jing-Yao Liu,[b] Zhifang Chai,[a,c] and Dongqi Wang[a]*

Received (in XXX, XXX) Xth XXXXXXXXX 20XX, Accepted Xth XXXXXXXXX 20XX

DOI: 10.1039/b000000x

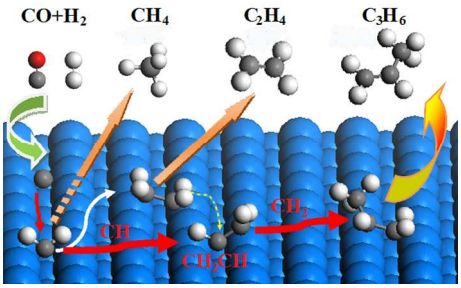

The activation of CO, hydrogenation of CH_x (x = 0–4) and C_2H_y (y = 0–5) species and the carbon chain propagation on V(100) were studied by means of periodic density functional theory (DFT) calculations. The results indicate that the activation of CO is very facile on V(100) via the direct dissociation rather than H-assisted pathways. The hydrogenation of CH_x/C_2H_y (except for CC) and the C–C coupling elementary steps are thermodynamically and kinetically unfavorable. The energy barriers to the former reactions are lower than those to the latter ones. The high coverage of reactants and the entropic effect may be the dominant factors responsible for the hydrogenation and carbon chain propagation. The simple microkinetic model built on the basis of the above results shows that CH_2 is the dominant CH_x species on the surface in the temperature range of 300-800 K. Starting from high coverage of CH_2, the building block of C-chain, CH_2CH_2 forms via coupling reaction and then desorbs from the surface. CH_2CH, appearing as the precursor, mainly forms from the coupling of CH_2 + CH followed by CH_2 insertion leading to CH_2CHCH_3. Although CH is more likely responsible for the chain propagation than CH_2 in view of energy barriers, its contribution suffers from its low coverage at considered conditions. These results are in good agreement with the experimental results.

Introduction

As a typical catalytic process to produce hydrocarbons via hydrogenation of CO, Fischer-Tropsch (F-T) synthesis has been widely investigated since being discovered in 1923,[1] and its importance is recognized once again with the increase of worldwide energy demand and environmental constraints in recent years. To find and design catalysts with better activity and selectivity, knowledge of the reaction mechanism is desirable.

Extensive experimental studies have been carried out on a variety of transition metal surfaces, and the carbene mechanism of Fischer and Tropsch,[2, 3] which proposes that the alkyl chain growth proceeds via CH_2 insertion following the dissociation of CO, is widely accepted.[4-11] Generally, the activation of CO is more facile on the early transition metals than on the late ones, while the case of the carbon coupling is opposite.[12] However, the mechanism remains to be investigated and many issues are under debate, such as the activation of CO via the direct dissociation or H-assisted pathways, the chemical identity and the stability of the participating species, and the chain growth pathways.[9, 11, 13-15] Though knowledge on the relative stabilities of various intermediates involved in the early steps of F-T process and the relevant potential energy surface is crucial to fully understand the F-T mechanism, it is difficult to obtain experimentally.

The development of advanced computational models and the growing computational power in recent years makes it feasible to study the mechanism of heterogeneous catalytic reactions by using the first-principles methods[16] and many theoretical works related to F-T process were carried out on a wide range of commonly used catalysts such as Fe,[17-24] Co,[12, 19, 24-28] Ni[13, 29] and Ru,[12, 20, 24, 30-32] as well as other potential metallic catalysts, e.g. Rh,[20, 24, 32-35] Pt,[36, 37] Pd.[33, 38] These studies show that the reaction mechanism displays strong dependence on the nature of metal surfaces. For CO activation, the H-assisted mechanism is proved more favorable than the direct dissociation on Fe and Co.[22, 27] For the path C→CH→CH_2→CH_3→CH_4, the largest activation energy corresponds to hydrogenation reaction of CH_2 on

Fe(100),[17] while the last step was considered as rate-determining at defects on studied Rh, Co, Ru, Fe and Re surfaces and an increase in the binding strength of C + 4H to the surface may suppress the production of methane.[24] The RC + C (R=alkyl or H) and CH + CH pathways occurring on Ru and Rh surfaces was suggested to be responsible for F-T chain propagation, while on the Fe surface, the pathway of C + CH_2/CH_3 may dominate, and on the Re surface C + CH does the job. When Co catalysts were employed, CH_2 + CH_2 and CH_3 + C appear more important, and the coupling reactions of RC + C and RC + CH also contribute to the chain growth on Co after CH_x coupling in addition to the pathways of RCH + CH_2 and RCH_2 + C.[16, 20, 24, 32]

A recent work by Shen and Zaera[39] studied the hydrocarbon chain growth on V(100) starting from CH_2I_2 and provided experimental evidence to identify CH_2CH as a plausible chain-propagation intermediate which may work as a precursor to produce CH_2CHCH_3 by coupling with CH_2. However, the information obtained from experimental work is limited and many fundamental issues concerning the mechanism and the selectivity remain to be solved. As far as we known, there is no theoretical study of the F-T process on V(100) until now. Herein, DFT and microkinetic modeling methodologies were employed to investigate the reaction mechanism of the F-T process on V(100), which covers the activation of CO, the adsorption stability of intermediate species and the possible pathways for chain growth from CH_x to C_2H_y and C_3H_z.

Computational Details

In this work all calculations were carried out with the Vienna ab initio simulation package (VASP).[40, 41] The projector augmented wave (PAW)[42, 43] method was used to describe ion-electron interactions and plane-wave basis set with an energy cutoff of 400 eV was used to expand the one-electron wave function. The Perdew-Burke-Ernzerhof (PBE)[44] functional within the generalized gradient approximation (GGA) was used to describe the electron correlation. Spin polarization was considered in all calculations. Geometries were relaxed using the conjugate gradient algorithm until the forces on all unconstrained atoms were smaller than 0.04 eV/Å. As described in our earlier work,[45] a (2 × 2 × 1) supercell cell with a five-layered periodic slab separated by a vacuum region of 15 Å was used to model the V(100) surface. The three lower layers were fixed and the two upper ones were allowed to relax. The calculations were performed with (6 × 6 × 1) Monkhorst-Pack k-point.

The climbing-image nudged elastic band (CI-NEB) method[46, 47] was used to search the transition states (TSs). The nature of each optimized structures, both minima and TSs, was identified by vibrational analysis, from which zero-point energy (ZPE) corrections were obtained and included in the barrier and reaction energy calculations. The adsorption energy (E_{ads}) for each possible adsorbate was calculated according to the following equation:

$$E_{ads} = E_{gas\text{-}surf} - (E_{surf} + E_{gas})$$

where $E_{gas\text{-}surf}$, E_{surf} and E_{gas} are the total energies of the surface with adsorbed species, the clean surface and the gas-phase species, respectively. The energy barrier for the bimolecular reaction was calculated relative to the energy of the infinite separation state. To evaluate the effect of van de Waals interaction on the adsorption and the kinetics of species on the metal surface, several key points were checked by an empirical dispersion correction using DFT-D3(BJ) method.[48,49]

Results and Discussion

Various configurations of CO, CH_x and C_2H_y, the most important species in the F-T synthesis, at three adsorption sites on V(100) (top, bridge and hollow as shown in Figure 1) were considered, and only the most stable ones are discussed here. For each elementary step we have investigated several possible reaction paths, and here only those with the minimum energy are reported.

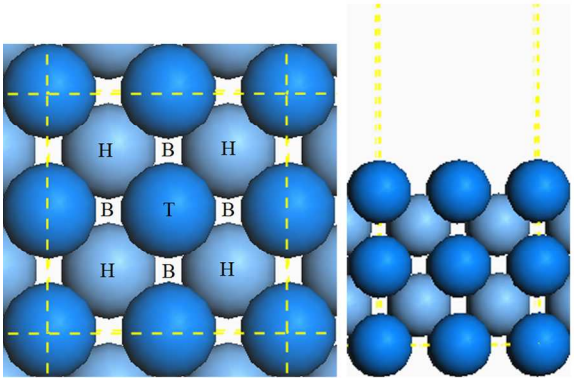

Fig. 1 Top (left) and side (right) views of the V(100) surface. The three possible adsorption sites of adsorbates at 0.25 ML, i.e. hollow, bridge and top sites, are labeled H, B and T, respectively. The light blue and navy blue spheres represent the even and odd layers of V atoms, respectively.

The activation of CO and H_2

The direct dissociation of CO is found facile on the V(100) surface. As described in our earlier work, [45] the adsorption of CO prefers to the hollow site and tiled from the surface, which assists its direct dissociation. The adsorption energy is -3.28 eV including ZPE and the value is calculated to be -3.60 eV with VDW-D3 correction in this work. The calculated energy barrier is as low as 0.33 eV (0.36 eV without ZPE and 0.37 with dispersion correction). In the transition state of the dissociation reaction, the C-O bond stretches to 1.83 Å from 1.14 Å, beyond which the O atom moves to the neighbor hollow site while the C atom stays at its binding site. This step is highly exothermic by 2.20 eV (see Figure 2).

It's known that the activation of CO on most metals is via its hydrogenation to CHO and/or COH,[22,27] however, on V(100), both hydrogenation steps are calculated to be endothermic by 0.60 and 1.41 eV, respectively, and the energy barrier for the former step is 0.90 eV, thus much less favorable than the direct dissociation. The dissociation of H_2 is barrierless and strongly exothermic on V(100). Following the initial dissociation of CO and H_2, other C-chain growth and hydrogenation steps may occur and will be discussed in detail in the next sections.

The adsorption and hydrogenation of CH_x

Both C atom and CH radical prefer to adsorb at the hollow site, with C interacting with four V atoms of the first layer (V_I) and one V atom of the second layer (V_{II}), and for CH radical the C–H bond (1.11 Å) is found to be perpendicular to the surface (see

Cite this: DOI: 10.1039/c0xx00000x

www.rsc.org/xxxxxx

ARTICLE TYPE

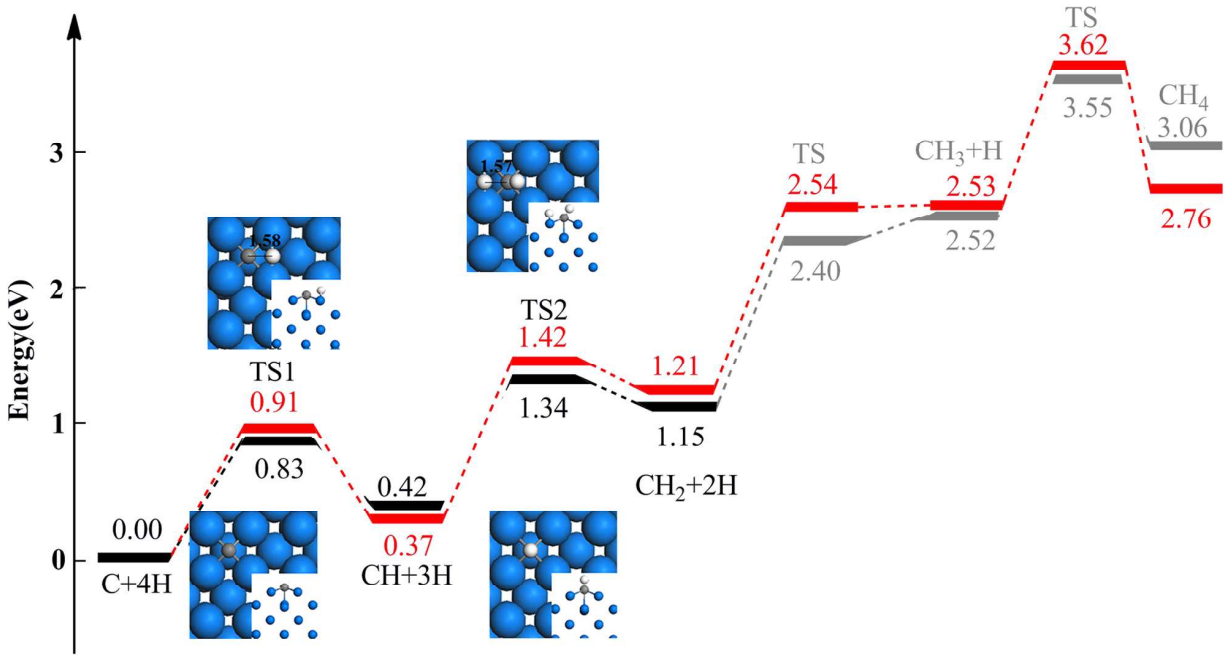

Fig. 2 Energy profile including ZPE correction (black) and also the vibrational entropy correction at 500 K (red) for the hydrogenation of CH_x (x = 0–3). The data of the hydrogenation of CH_2 and CH_3 (in gray) are from ref.45. The gray and white spheres represent C and H atoms, respectively.

Figure 2). The bond lengths of C–V_I and C–V_{II} are 2.05 and 2.10 Å, respectively in the case of C atom, and 2.16 and 2.10 Å in the case of CH radical. The longer distance between CH radical and V_I is consistent with the smaller adsorption energy of CH than that of C on the surface (-7.84 versus -8.95 eV), suggesting a weaker interaction between the CH radical and the surface than that for the adsorbed C atom. The adsorption of CH_x (x = 2–4) species has been studied in previous work,[45] and an adsorption energy of –8.20 eV for CH_2, which is close to that of C and CH, and of –2.17 eV for CH_3 was reported, indicating the highest mobility for CH_3 while the least for C atom. The adsorption energy of CH and CH_2 including dispersion correction is calculated to be -8.11 and -8.60 eV, respectively. Meanwhile, the adsorption of CH_3 at the bridge site was found to be more stable than at the hollow site. CH_4 is only weakly physisorbed on the surface. These results are similar to those on other surfaces.[17, 18, 34]

The potential energy profile for the hydrogenation of C atom to produce methane in a stepwise manner is plotted in Figure 2 (the black one) and the PES curve including vibrational entropy term using the harmonic approximation (see the supporting information) at 500 K is also given (the red line). Both of the hydrogenation of C and CH are endothermic by 0.42 and 0.73 eV, respectively. During the reaction, C (or CH) remains at the hollow site, and the H atom moves to it by overcoming a barrier of 0.83 (0.92) eV. The value without ZPE is 0.91 (0.91) eV and becomes 0.92 (0.93) including dispersion effects. The C-H bond length in the transition states (TS1 and TS2) are similar, 1.58 and 1.57 Å, respectively. According to our earlier study,[45] the subsequent hydrogenation of CH_2 and CH_3 was found to be also endothermic (1.37 and 0.54 eV, respectively) with energy barriers of 1.25 and 1.03 eV, respectively, and the diffusion of H atoms is facile on V(100), which benefits the hydrogenation of CH_x. These results indicate that all elementary reaction processes starting from C to produce CH_4 are endothermic, leading to an overall endothermicity of 3.06 eV. The largest energy barrier corresponds to the third step, CH_2 hydrogenation, similar to that on Fe(100) with an energy barrier of 0.86 eV.[17]

In order to take into account the influence of temperature on chemical behavior of some adsorbed species, AIMD simulations on the adsorbed CH_2 was carried out at three temperatures of 300, 500 and 800 K respectively for more than 20 ps each. Figure S1 shows how the C–H bond of CH_x evolves during AIMD simulation at 300 and 800 K with nearest image convention imposed.

As seen in Figure S1a, on the clean V(100) surface, we didn't observe the dissociation of CH_2 during the simulation at 300 K, which is the case at 500 K. At 800 K, as seen in Figure S1b, the dehydrogenation of CH_2 was observed. The leaving H atom first moved to the adjacent hollow site, then moved to the diagonal hollow site, but the yielded CH did not dissociate. These results indicate that the dissociation of CH is more difficult than that of CH_2, which is consistent with the higher energy barrier.

In order to investigate the influence of surface H atoms,

a simulation of CH_2 at 800 K was carried out with an H atom adsorbed at the diagonal hollow site (see Figure S1c). The presence of the H atom was found to have little effect on the dissociation of CH_2, but do limit the motion of the released H atom and lead to its immobilization at the adjacent hollow site.

These results indicate that the dissociation of CH_2 and CH may be difficult on the V(100) surface under considered condition, thus may appear with long lifetime and lager coverage, which is verified by the microkinetic model, as discussed in the latter section. CH_3 is much less stable for two reasons: on one hand, it is easy to dissociate, and on the other hand, its hydrogenation gives CH_4, which may desorb from the surface easily.

The adsorption, formation and hydrogenation of C_2H_y on V(100)

Starting from CH_x species, the C–C coupling reaction initiates the chain propagation, and there is no doubt that C_2H_y are important intermediates. To better understand the chain growth mechanism, in this section, we first discussed the adsorption of C_2H_y species, followed by the investigation of all possible C–C coupling reactions that produce C_2H_y species and their hydrogenation on V(100).

Adsorption of C_2H_y. The most stable structures, selected geometric parameters together with the adsorption energies are shown in Figure 3 and Table 1. Most C_2H_y species have similar configurations except for CH_2CH_2 and CH_2CH_3 (see Figure 3). In these configurations, the C atom baring less H atoms (denoted as C1) sits above a hollow site and interacts with four V_I and one V_{II} atoms, similar to CH_x (x = 0–2), and another C atom (C2) locates at the adjacent bridge site and binds with two V_I atoms. Such trends are similar to that on Pt(110).[36]

In general, shorter C–V bond means stronger binding. The C1–V_I bond in CH_xC (x = 0–3) is the shortest with values of 2.07, 2.08 and 2.09 Å for CH_2C, CHC and C_2, and 2.15 Å for CH_3C respectively. The bond length becomes longer when going to CH_xCH (x = 1–3), which is around 2.19 Å. The C1–V_{II} bond length is the shortest in CC, CHC and CH_3C (2.13 Å) and is around 2.16–2.19 Å in other C_2H_y species. The distance of C2–V_I in CH_xC (x = 0–3) increases with the number of H atoms (1.97<2.05<2.19<2.47 Å), and this is also the case for CH_xCH (x = 1–2) (2.02<2.15<2.50 Å).

For all species, the C–C bond is tilted from the surface with the bridge C farther from the V(100) surface, and the distance between the two C atoms increases with the number of H atoms on C2 atom (C–CH_x (x = 0–3): 1.40<1.43<1.46<1.51 Å; CH–CH_x (x = 1–3): 1.47<1.48<1.53 Å). Same trend is observed for the angle of the C–C bond tiled from the surface (C–CH_x (x = 0–3): 35.94<37.23<41.69<55.19°; CH–CH_x (x = 1–3): 29.64<35.02<50.69°) and the C–H bond length of CH fragment in CHCH, $CHCH_2$ and $CHCH_3$ (1.16<1.18<1.20 Å). The configuration of CH_2CH_2 has been described in our earlier work.[45] CH_2CH_3 adsorbs on V(100) with CH_2 located at the bridge site, which is different from other C_2H_y species, with a C–C bond length of 1.53 Å, C–V of 2.25 Å and an angle of 39.76°.

A correlation between the adsorption stability of most C_2H_y on V(100) and the C1–V distance and the number of H atom on the C atom bound with the surface may be deduced from the data in Table 1: the shorter the C1–V distance or the less saturated the C atom, the stronger the binding. Among all C_2H_y species, the adsorption of C_2 is the most exothermic by –8.62 eV. In the case of CHC and CH_3C, the energies decrease to –6.87 and –6.77 eV, respectively. The exothermicity is even less for CH_2C which is around –5.67 eV, and for the CH_xCH species, which are –4.83, –4.28 and –3.49 eV for CHCH, CH_2CH and CH_3CH, respectively, suggesting the stability of CH_xCH on V(100) decreases with the number of H atom on the C2 atom. The adsorption energy of CH_3CH_2 is –1.85 eV, and CH_2CH_2 is found only weakly bound to the surface with an adsorption energy of –0.57 eV, thus it is likely to desorb from the surface.[45] The adsorption energy including dispersion correction is calculated to be -4.87 and -1.92 eV for CH_2CH and CH_2CH_2, respectively.

In brief, CH_xCH_y ($y \geq x$) have preferred adsorption modes with less saturate C atom bound on the surface rather than other configurations, and the adsorption sites are similar to the corresponding CH_x species. For the isomers, the configuration with less saturate C1 is more stable in view of adsorption energy on the surface, e.g. the binding of CH_2C, CH_3C and CH_3CH are stronger than CHCH, CH_2CH and CH_2CH_2, respectively, similar to that on Fe(100).[18]

Table 1. The adsorption energies (E_{ads}, in eV) and geometric parameters (distance in Å and angle in degree) of the most stable C_2H_y on V(100)

Species	Configurations	$d_{C1–VI}$ [(a)]	$d_{C1–VII}$	$d_{C2–VI}$	Angle [(b)]	$d_{C1–C2}$	E_{ads}
CC	C1-hollow, C2-bridge	2.09	2.13	1.97	35.94	1.40	–8.62
CHC	C1-hollow, C2-bridge	2.08	2.13	2.05	37.23	1.43	–6.87
CH_3C	C1-hollow, C2-bridge	2.15	2.13	2.47	41.69	1.51	–6.77
CH_2C	C1-hollow, C2-bridge	2.07	2.16	2.19	55.19	1.46	–5.67
CH_3CH	C1-hollow, C2-bridge	2.19	2.19	2.50	50.69	1.53	–4.83
CH_2CH	C1-hollow, C2-bridge	2.19	2.21	2.15	35.02	1.48	–4.28
CHCH	C1-hollow, C2-bridge	2.18	2.18	2.02	29.64	1.47	–3.49
CH_3CH_2	C1-bridge, C2-hollow	2.25	–	3.27	39.76	1.53	–1.85
CH_2CH_2 [(c)]	C1-hollow, C2-bridge	2.32	2.52	2.23	20.82	1.51	–0.57

[(a)] C1 refers to the C atom with less H atoms. [(b)] The angle of the C–C bond tiled from the surface. [(c)] Data from ref. 45

Cite this: DOI: 10.1039/c0xx00000x

www.rsc.org/xxxxxx

ARTICLE TYPE

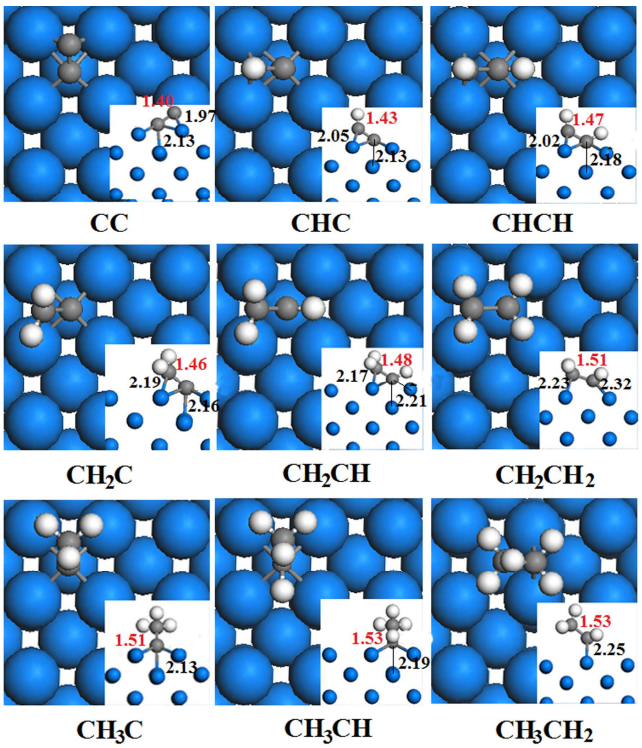

Fig. 3 The most stable structures of C_2H_y on V(100). The C–V bond lengths (in Å) are given in black and the C–C bond lengths (in Å) in red.

C–C coupling. C–C coupling reaction may occur between two adsorbed CH_x close to each other and the transition states were shown in Figure 4. As mentioned above, CH_x radicals with more H atoms bind relatively weaker to the surface, and it is easier for these species to diffuse on the surface towards those CH_x with less H atom in the coupling processes. For example, to approach to the transition state for the coupling of CH_2 and CH, TS8, the adsorbed CH_2 migrates toward the CH group and the activated CH remains at its initial hollow site. TS8 is similar to that on Co and Ru surfaces in the presence of a multi-centered bond.[12]

The nascent C–C bond lengths in the TSs are also shown in Figure 4 and all of them are around 2.00 Å. In the transition states for the coupling reactions of C atom with CH_x (x=0-3), TS3–TS6, the forming C–C bond lengths are 1.80<1.92<1.97<2.07 Å, respectively. For the coupling of CH with CH_x (x=1-3), these values in TSs7–9 are 1.92<1.95<2.04 Å, respectively. When going to more saturated CH_x species, i.e. the coupling reactions of CH_2 with CH_3 and CH_2, the values become even longer to 2.08 and 2.09 Å in TS10 and TS11, respectively. It is clear that the length of the forming C–C bond is related to the unsaturation of the CH_x fragment, similar to that in C_2H_y species.

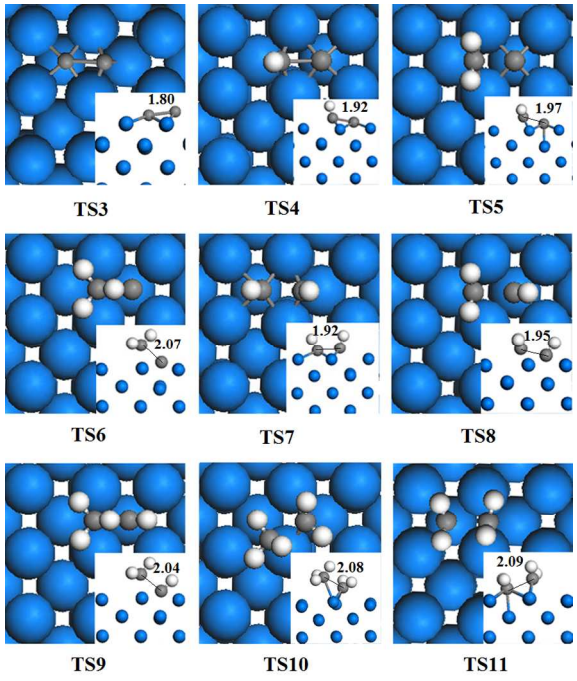

Fig. 4 The TS structures (in Å) of the C–C coupling on V(100).

In view of energy barriers (see Figure 5), the coupling paths studied here may be classified into three groups. The first group includes the CH_3 + C and CH_3 + CH coupling reactions, which are inherent with the lowest barriers of 1.05 and 1.28 eV, respectively, which may be resulted from the participation of the relatively highly diffusive CH_3 in the reactions. The coupling reactions with moderate difficulty constitute the second group, including the paths of C + CH, C + CH_2, CH + CH and CH + CH_2 with similar energy barriers of 2.02, 1.97, 2.00 and 2.03 eV, respectively, which is because the diffusion ability of CH and CH_2 is similar and much weaker than CH_3 involved in the first group. The values without ZPE for the CH+CH and CH+CH_2 are 1.85 and 1.95 eV, which become 1.84 and 1.99 including dispersion correction. The reactions with the highest energy barriers belong to the third group, i.e. the coupling reactions of C + C, CH_2 + CH_2 and CH_2 + CH_3, the barriers of which are 2.70, 2.71 and 2.49 eV, respectively. In this group, either it is hard for both reactants to migrate (C + C) or significant repulsive interaction is present between the two reactants, which makes it difficult for the coupling reactions to happen. These results reflect the composite effect of the diffusion ability of the migrating CH_x and the repulsive interaction between the radical pair. Overall, for the radical pair that with the less repulsive interaction and/or higher diffusion ability, the barrier to overcome is lower, and the lowest value is obtained to the C + CH_3 coupling reaction, which is same as that on Fe and Co surface.[19]

Cite this: DOI: 10.1039/c0xx00000x

www.rsc.org/xxxxxx

ARTICLE TYPE

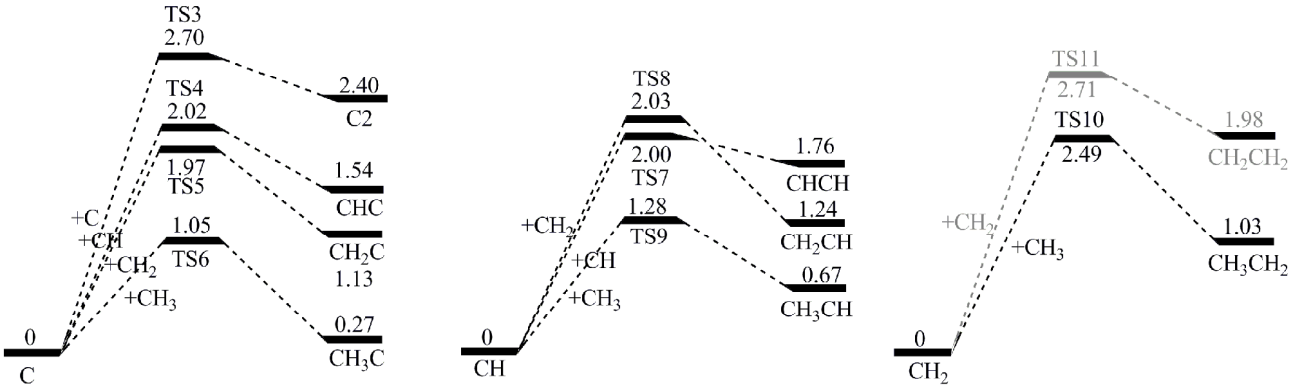

Fig. 5 Energy profile for the C–C coupling steps (in eV). The coupling of CH_2 (in gray) is from ref.45

In addition, we note that for coupling reactions C + CH_x, the reaction energy barriers correlate with the lengths of the partially formed C–C bond in the TSs, i.e. the longer the C–C bond length, the lower the energy barrier. This, together with the correlation between the C–C bond length, the diffusion ability and the unsaturation of the CH_x fragment mentioned above, shows that it is possible that these reactions are determined essentially by unsaturation of the CH_x.

All of the coupling reactions studied here are endothermic and the strongest endothermicity was found in the reaction between the C + C radical pair with a value of 2.40 eV. It decreases to 1.76, 1.54, 1.24 and 1.03 eV, respectively for the reactions of CH + CH, CH + C, CH + CH_2 and CH_2 + CH_3, and the lowest value (0.27 eV) is for C + CH_3 . It is clear from Figure 5 that, for the coupling reaction of C with CH_x, the step with lower energy barrier appears with smaller endothermicity, which is same as the case for CH (or CH_2) with CH_x, except for the CH + CH step.

The diffusion ability of CH_3 makes the coupling steps CH_3 + C (or CH) more favorable both in view of kinetics and thermodynamics. According to our calculations, the effective energy barriers, which is defined as the energy difference between the highest transition state (TS) and the C+*y*H species, increase in the order CH + CH < C + CH < C + C < C + CH_2 < CH + CH_2 < C + CH_3 < CH + CH_3 < CH_2 + CH_2 < CH_2 + CH_3 with the values 2.42 < 2.64 < 2.70 < 3.12 < 3.18 < 3.57 < 3.80 < 3.86 < 5.01 eV. On the surface of V(100), C is the most stable species and its hydrogenation and coupling reactions are endothermic, thus by referring to the energy of the thermodynamically most stable species, it is clear that, all C-C coupling steps are more difficult to happen than the formation of CH_2 (1.34 eV) in energy barriers.

Hydrogenation of C_2H_y. In order to evaluate the propensity of the transformation of C_2H_y species discussed above, all potential hydrogenation pathways of C_2H_y were investigated here. The energy barriers and reaction energies of these reactions, together with those of all C–C coupling steps mentioned above are collected in Figure 6, and the configurations of transition states are shown in Figure 7 with the newly formed C–H bond length given. Since the direct 1,2-H shift have been proven difficult in previous studies,[37, 38] they were not studied in this work. In this section, the stepwise hydrogenation steps starting from the C_2 species, followed by the possible pathways in F-T process, were discussed.

The data in Figure 6 indicate that most hydrogenation processes of C_2H_y are endothermic except for the step C_2 + H → C_2H which is exothermic by 0.45 eV with an energy barrier of 0.72 eV. The hydrogenation of C_2H may produce CH_2C or CHCH, which are endothermic by 0.32 and 0.64 eV, respectively, and the corresponding energy barriers are 0.75 and 0.81 eV. The highly unsaturated CH_2C may be reduced further to CH_2CH or to CH_3C by overcoming an energy barrier of 0.78 or 0.89 eV and both are

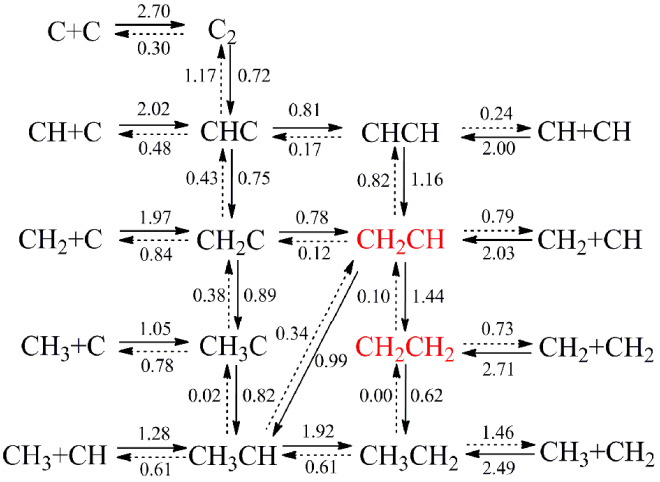

Fig. 6 Paths of C–C coupling reactions to produce C_2H_y species and the subsequent hydrogenations. ZPE correction is included in the energy barrier (in eV) of each path.

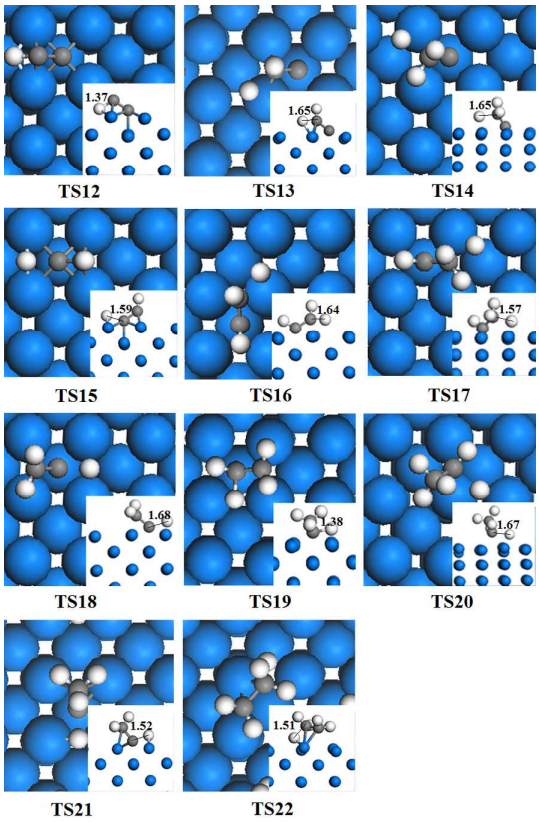

Fig. 7 The TS structures of the hydrogenation of C_2H_y on V(100) with the newly formed C–H bond length in Å.

endothermic by 0.66 and 0.51 eV respectively. In principle, CH_2CH may be also produced via the hydrogenation of CHCH with a higher barrier of 1.16 eV. The further hydrogenation of CH_3C and CH_2CH gives CH_3CH, both of which are calculated to be endothermic by 0.80 and 0.65 eV, and the barriers are 0.82 and 0.99 eV, respectively. A second path for the hydrogenation of CH_2CH is to reduce the less saturated C1 atom and give ethylene molecule (CH_2CH_2) with a much higher energy barrier of 1.44 eV and strong endothermicity by 1.34 eV. The subsequent hydrogenation of both CH_3CH and CH_2CH_2 gives CH_3CH_2, with an energy barrier of 1.92 eV to the former compared to a lower value of 0.62 eV to the latter (Figure 6).

Starting from the C + H to form CH_2CH_2, the effective energy barrier to the path via the coupling of CH_2 is smaller than the other paths since the hydrogenations of CH_2CH and CHCH are endothermic and face high energy barriers, according to our calculations. This is in consistent with the experimental observations,[39] in which CH_2 appears as the reactant, and explains the formation of CH_2CH_2 via direct coupling reaction of two CH_2.

Regarding to the pathway for the formation of CH_2CH, according to our calculations, in addition to the direct coupling of CH_2 and CH, there may exist two other possibilities. The first one is the dehydrogenation of CH_2CH_2 which is inherent with a very low energy barrier (0.10 eV) and large exothermicity (1.34 eV), and the other one is a three-step process starting from CHCH, i.e. along the path CHCH → CHC → CH_2C → CH_2CH. In principle, the direct CHCH may also produce CH_2CH, however, its much higher effective energy barrier, which amounts up to 1.16 eV makes it uncompetitive against the stepwise pathway to which the E_{eff} is calculated to be 0.22 eV. Note that both pathways involve the dehydrogenation steps, low coverage of the surface is required to guarantee the availability of extra surface site, otherwise the dissociation steps may be blocked.

Microkinetic model

On the basis of our DFT calculations, a 16-step microkinetic model was developed to further investigate the coverage and the role of CH_x and C_2H_y species under the typical experimental condition (P_{co} = 4 atm, P_{H2} = 8 atm and T = 300-800 K) on V(100). In this work, we focus on discussing the C-chain growth on clean V(100) and the effect of oxygen was not studied. Thus the simple microkinetic model corresponding to a very low O* coverage (θ_O = 0) is given and the effect of the coverage of surface species on the adsorption energy of CO and H_2 was neglected. The elementary steps and the corresponding energy barriers and reaction energies were shown in Table 2. Typical pre-exponential factors of 10^{13} s^{-1} were used.[50] The details about the microkinetic modelling are given in the Supporting Information and the results are collected in Table S1 and S2.

Table 2. Calculated activation barriers and the reaction energy including ZPE for elemental steps.

	Surface reactions	E_f(eV)	ΔH(eV)
1	CO (g) + * ↔CO*		-3.28
2	H_2 (g) + 2* ↔2H*		-1.36
3	CO* + * → C* + O*	0.33	-2.20
4	C* + H* → CH* + *	0.83	0.42
5	CH* + H* → CH_2* + *	0.92	0.73
6	CH_2* + H*↔ CH_3* + *	1.37	0
7	CH_3* + H* → CH_4 (g) + 2*	1.03	0.54
8	C* + C* ↔ C_2* + *	2.70	2.40
9	C* + CH* ↔ CCH* + *	2.02	1.54
10	C* + CH_2* ↔ CH_2C* + *	1.97	1.33
11	C* + CH_3* ↔CH_3C* + *	1.05	0.27
12	CH* + CH* ↔ CHCH* + *	2.00	1.76
13	CH* + CH_2* ↔ CH_2CH* + *	2.03	1.24
14	CH* + CH_3* ↔ CH_3CH* + *	1.28	0.67
15	CH_2* + CH_2* ↔ CH_2CH_2* + *	2.71	1.98
16	CH_2* + CH_3* ↔ CH_3CH_2* + *	1.46	1.03

An asterisk represents a free site on the surface.

Our results show that, under the studied condition, CH_2 is the dominant CH_x surface species in the whole temperature range (300-800 K) (see Table S1). However, when the dissociation of CH_2 becomes possible (step 5r) and is included in the model at high temperature of 800 K, CH coverage becomes the highest, followed by that of CH_2. This suggests that both CH_2 and CH are important CH_x species responsible for the C-chain growth in the considered temperature range 300-800 K, consistent with the above discussion.

The forward reaction rate of CH_2+CH, CH_2+C and CH_3+C coupling top the other channels from 300 to 800 K and the CH_2CH, CH_2C and CH_3C coverage are the highest among all C_2H_y species except CH_2CH_2 and CH_2CH_3 (see Table S2). It is noted that the desorption of CH_2CH_2 and CH_3CH_2 by hydrogenation were not considered in the model which may

decrease the coverage of these two species. If the step 5r is included in the model at 800 K, the forward reaction rate of CH_2+ CH tops the other channels and both CH_2CH and CHCH become dominant as a consequence of the higher coverage of CH than that of CH_2. Thus at experimental temperature, CH_2CH is the important C_2H_y species and may be responsible for the C-chain growth.

In summary, CH_2 is the most possible reactant for the C-C coupling reaction because of its high coverage, and CH is also recognized as a highly possible species responsible for the C-C coupling in view of energy barrier while its significance may be limited by its lower coverage at experimental temperature. Starting from the high coverage of CH_2, the reaction of CH_2+CH_3 is most favourable, but the formed CH_2CH_3 will be desorption from the surface after hydrogenation. The reaction CH_2 + CH_2 to CH_2CH_2 desorbing from the surface may be also favourable although need overcome a high energy barrier of 2.71 eV. The other reactions with lower effective energy barriers such as CH + CH and CH + CH_3 seem possible, but the much lower coverage of CH and CH_3 make them much less competitive than CH + CH_2. Thus, CH_2CH may be the most possible C_2H_y species from the C-C coupling on V(100) responsible for the C-chain growth in considered condition, as proven in Shen's experiment.[39]

The formation of C_3H_z on V(100)

The further chain growth reactions are more complicated concerning the possibility for multiple CH_x and C_2H_y species to co-exist on the surface. Here we limited our calculations on two reactions based on the thermostabilities of the CH_x and C_2H_y building blocks: (1) CH_2CH reacts with the CH_2 to from CH_2CHCH_2 by overcoming a barrier of 2.60 eV (ZPE correction not included), (2) CH_2CH reacts with CH to form CH_2CHCH by overcoming a barrier of 2.04 eV, followed by a further hydrogenation step to give CH_2CHCH_2 after passing a barrier of 0.69 eV. The reaction energies of the three steps are 1.22, 1.09 and 0.69 eV, respectively. The terminal CH_2 group of the newly formed CH_2CHCH_2 can abstract an H atom from the neighboring binding site and produce CH_2CHCH_3, which may then desorb from the surface. The barrier and the reaction energy for this step is 1.31 and 0.86 eV, respectively. These results show that CH displays higher reactivity than CH_2 in the C-C coupling reactions towards the formation of CH_2CHCH_2, as implied by the lower energy barrier to the second path than to the first one (2.60 versus 2.04 eV).

However, as discussed above, the reactions that require the participation of CH suffer from the low coverage of CH compared to that of CH_2 at experimental temperature, which nevertheless benefits the coupling between CH_2CH and CH_2. This suggests that CH_2 may be responsible for the C-chain growth to form the dominant C_3H_z product via the path $CH_2CH \rightarrow CH_2CHCH_2 \rightarrow CH_2CHCH_3$, which agrees with the speculation in Shen's experiment.[39]

Conclusions

In this work, the activation of CO, hydrogenation of CH_x and C_2H_y, as well as the C–C coupling process were studied by periodic DFT. The results indicate that CO and CH_x (x = 0–2) prefer to locate at the hollow site on V(100). Most C_2H_y species prefer to adsorb at the hollow site through the less saturated C atom and another C atom at the bridge site, with an exception that CH_3CH_2 binds at the bridge site through its CH_2 moiety. The adsorption strength of the CH_x and C_2H_y species is related to the extent of their unsaturation. The binding strength of CH_x is relatively strong on the surface, which does not facilitate their diffusion on the surface.

The activation of CO is facile via the direct dissociation rather than H-assisted pathways on V(100). The hydrogenation of CH_x, C_2H_y (except CCH) and the C–C coupling reactions are all kinetically and thermodynamically unfavorable and their occurrence depends on the high coverage of reactants and entropy effect. For the C-C coupling steps, the larger the difference in the saturation of the two C atoms, the more favorable the reactions are both in terms of thermodynamics and kinetics.

In F-T synthesis, starting from the reactants of C + H on the surface, CH_2 may be the dominant CH_x species at experimental temperature. Starting from high coverage of CH_2, CH_4 may form from its hydrogenation and desorbs from the surface as the CH_x product at high H coverage. C_2H_4 forms from its direct coupling and desorbs from the surface and the key chain-propagation intermediate, CH_2CH, comes from the its coupling with CH. Both the coupling steps and the continue coupling of CH_2CH with CH or CH_2 leading to the product CH_2CHCH_3 are unfavorable kinetically and thermodynamically. Note that, van de Waals interaction may increase the adsorption energies of hydrogen-containing species which may be enhanced as chain grows,[16,22] but the effect on the energy barrier of reaction on the metal surface is negligible. The high coverage of CH_x and H and the entropic effect may appear as the dominant factor responsible for the C-chain growth as well as the hydrogenation, and the contribution of CH may be limited by the its low coverage compared to that of CH_2 although the reactions involved CH with lower energy barriers. The results are in good agreement with the experimental results.[39] The whole process can be described as follows:

$$CO\ (g) + * \rightarrow CO* \quad (1)$$
$$H_2\ (g) + 2* \rightarrow 2H* \quad (2)$$
$$CO* + * \rightarrow C* + O* \quad (3)$$
$$C* + H* \rightarrow CH* + * \quad (4)$$
$$CH* + H* \rightarrow CH_2* + * \quad (5)$$
$$CH_2* + H* \rightarrow CH_3* + * \quad (6)$$
$$CH_3* + H* \rightarrow CH_4\ (g) + 2* \quad (7)$$
$$CH_2* + CH_2* \rightarrow C_2H_4* + * \quad (8)$$
$$C_2H_4* \rightarrow C_2H_4\ (g) + * \quad (9)$$
$$CH_2* + CH* \rightarrow CH_2CH* + * \quad (10)$$
$$CH_2CH* + CH_2* \rightarrow CH_2CHCH_2* + * \quad (11)$$
$$CH_2CHCH_2* + H* \rightarrow CH_2CHCH_3* + * \quad (12)$$
$$CH_2CHCH_3* \rightarrow CH_2CHCH_3\ (g) + * \quad (13)$$

Acknowledgments

This work was financially supported by the National Natural Science Foundation of China to Z.Chai (No. 91026000), to J.Liu (Nos. 20973077 and 21373098), to D.Wang (No. 91226105), by the Chinese Academy of Sciences in the framework of a Frontier of Novelty program to D.Wang (No. Y2291810S3), and by the Program for New Century Excellent Talents in University (NCET) to J.Liu, which are gratefully acknowledged.

Calculations were done on the computational grids in the computer center of the Institute of High Energy Physics (IHEP) maintained by Drs. Jingyan Shi and Bowen Kan, in the Supercomputing Center of Chinese Academy of Sciences (SCCAS) and in the National Supercomputing Center in Tianjin (NSCC-TJ).

Notes and references

[a] *CAS Key Laboratory of Nuclear Radiation and Nuclear Energy Techniques, and Multidisciplinary Initiative Center, Institute of High Energy Physics, Chinese Academy of Sciences, Beijing 100049, China. E-mail: dwang@ihep.ac.cn*

[b] *Institute of Theoretical Chemistry, State Key Laboratory of Theoretical and Computational Chemistry, Jilin University, Changchun 130023, China*

[c] *School of Radiation Medicine and Interdisciplinary Sciences (RAD-X), Soochow University, Suzhou 215123, China*

1 F. Fischer, H. Tropsch, *Brennst. Chem.* 1923, **4**, 276.
2 F. Fischer, H. Tropsch, *Brennst. Chem.* 1926, **7**, 97.
3 F. Fischer, H. Tropsch, *Chem. Ber.* 1926, **59**, 830.
4 M. A. Vannice, *J. Catal*. 1975, **37**, 449.
5 C. A. Mims, L. E. Mccandlish, M. T. Melchior, *Catal. Lett.* 1988, **1**, 121.
6 K. R. Krishna, A. T. Bell, *Catal. Lett.* 1992, **14**, 305.
7 M. L. Turner, P. K. Byers, H. C. Long, P. M. Maitlis, *J. Am. Chem. Soc.* 1993, **115**, 4417.
8 H. C. Long, M. L. Turner, P. Fornasiero, J. Kašpar, M. Graziani, Maitlis, P. M. *J. Catal.* 1997, **167**, 172.
9 P. M. Maitlis, R. Quyoum, H. C. Long, M. L. Turner, *Appl. Catal. A: Gen.* 1999, **186**, 363.
10 R. M. Watwe, R. D. Cortright, J. K. Nørskov, J. A. Dumesic, *Catal. Today* 2002, **104**, 2299.
11 S. B. Ndlovu, N. S. Phala, M. Hearshaw-Timme, P. Beagly, J. R. Moss, M. Claeys, E. van Steen, *J. Am. Chem. Soc.* 2002, **71**, 343.
12 Q. Ge, M. Neurock, H. A.Wright, N. Srinivasan, *J. Phys. Chem. B* 2002, **106**, 2826.
13 H. Guo, F. Zaera, *Surf. Sci.* 2003, **547** (3), 299.
14 P. M. Maitlis, *J. Org. Chem.* 2004, **689** (24), 4366.
15 S. M. Davis, G. A. Somorjai, Hydrocarbon Conversion over Metal Surfaces. Interscience Publishers: New York, 1982.
16 J. Cheng, P. Hu, P. Ellis, S. French, G. Kelly, C. M. Lok, *Top. Catal.* 2010, **53** (5–6), 326.
17 D. C. Sorescu, *Phys. Rev. B* 2006, **73**, 155420.
18 J. M. H. Lo, T. Ziegler, *J. Phys. Chem. C* 2007, **111**, 13149.
19 M. Mavrikakis, A. A. Gokhale. Abstracts of Papers of the American Chemical Society, 2005, **229**, U861.
20 J. Cheng, P. Hu, P. Ellis, S. French, G. Kelly, C. M. Lok, *J. Phys. Chem. C* 2008, **112**, 6082.
21 C.-F. Huo, Y.-W. Li, J. Wang, H. Jiao, *J. Am. Chem. Soc.* 2009, **131**, 14713.
22 H.-J. Li, C.-C. Chang, J.-J. Ho, *J. Phys. Chem. C* 2011, **115** (22), 11045.
23 M. H. Mahyuddin, R. V. Belosludov, M. Khazaei, H. Mizuseki, Y. Kawazoe, *J. Phys. Chem. C* 2011, **115** (48), 23893.
24 J. Cheng, P. Hu, P. Ellis, S. French, G. Kelly, C. M. Lok, *J. Phys. Chem. C* 2009, **113** (20), 8858.
25 X.-Q. Gong, R. Raval, P. Hu, *Mol. Phys.* 2004, **102** (9–10), 993.
26 J. Cheng, X.-Q. Gong, P. Hu, C. M. Lok, P. Ellis, S. French, *J. Catal.* 2008, **254** (2), 285.
27 M. Zhuo, K. F. Tan, A. Borgna, M. Saeys, *J. Phys. Chem. C* 2009, **113**, 8357.
28 L. Xu, Y. Ma, Y. Zhang, B. Chen, Z. Wu, Z. Jiang, W. Huang, *J. Phys. Chem. C* 2011, **115** (8), 3416.
29 J. E. Mueller, A. C. T. van Duin, W. A. Goddard III, *J. Phys. Chem. C* 2010, **114**, 20028.
30 I. M. Ciobîcă, G. J. Kramer, Q. Ge, M. Neurock, R. A.van Santen, *J. Catal.* 2002, **212** (2), 136.
31 Z.-P. Liu, P. Hu, *J. Am. Chem. Soc.* 2002, **124**, 11568.
32 J. Chen, Z.-P. Liu, *J. Am. Chem. Soc.* 2008, **130**, 7929.
33 Z.-P. Liu, P. Hu, *J. Am. Chem. Soc.* 2003, **125**, 1958.
34 P. W. van Grootel, R. A. van Santen, E. J. M. Hensen, *J. Phys. Chem. C* 2011, **115** (26), 13027.
35 Y.-H. Zhao, M.-M. Yang, D. Sun, H.-Y. Su, K. Sun, X. Ma, X. Bao, W.-X. Li, *J. Phys. Chem. C* 2011, **115** (37), 18247.
36 A. T. Anghel, S. J. Jenkins, D. J. Wales, D. A. King, *J. Phys. Chem. B* 2006, **110**, 4147.
37 Z.-J. Zhao, L. V. Moskaleva, H. A. Aleksandrov, D. Basaran, N. Rösch, *J. Phys. Chem. C* 2010, **114**, 12190.
38 Z.-X. Chen, H. A. Aleksandrov, D. Basaran, N. Rösch, *J. Phys. Chem. C* 2010, 114, 17683.
39 M. Shen, F. Zaera, *Angew. Chem.* 2008, **47** (35), 6583.
40 G. Kresse, J. Hafner, *Phys. Rev. B* 1993, **47**, 558.
41 G. Kresse, J. Furthermüller, *Phys. Rev. B* 1996, **54**, 11169.
42 P. E. Blöchl, *Phys. Rev. B* 1994, **50**, 17953.
43 G. Kresse, D. Joubert, *Phys. Rev. B* 1999, **59**, 1758.
44 J. P. Perdew, K. Burke, M. Ernzerhof, *Phys. Rev. Lett.* 1996, **77**, 3865.
45 H. Wang, C.-Z. He, L.-Y. Huai, J.-Y. Liu, *J. Phys. Chem. C* 2012, **116**, 10639.
46 G. Henkelman, B. P. Uberuaga, H. Jónsson, *J. Chem. Phys.* 2000, **113**, 9901.
47 G. Henkelman, H. Jónsson, *J. Chem. Phys.* 2000, **113**, 9978.
48 S. Grimme, J. Antony, S. Ehrlich, S. Krieg, *J. Chem. Phys.* 2010, **132**, 154104.
49 S. Grimme, S. Ehrlich, L. Goerigk, *J. Comp. Chem.* 2011, **32**, 1456.
50 J. A. Dumesic, D. F. Rudd, L. M. Aparicio, J. E. Rekoske, A. A. Treviño, The Microkinetics of Heterogeneous Catalysis; American Chemical Society: Washington, DC, 1993; p 40.